RESEARCH

Bifunctional Luminescent Rare Earth Metal–Organic Frameworks for Highly Sensing Fe^{3+} Ions and TNP

Jiewei Rong[1] · Li Li[1] · Longde Wang[1] · Wenwei Zhang[2]

Abstract

Two isostructural rare earth metal–organic frameworks, namely $[Re_2(BBTC)(DMF)_5Cl_2]\cdot 2DMF\cdot H_2O$ $[BBTC^{4-} = 1,1'$-butadiynebenzene-3,3',5,5'-tetracarboxylate, $Re = Y$ (**1**) and Ho (**2**)], have been prepared via solvothermal reaction. Single crystal $X-$ray analyses reveal that complexes **1** and **2** both crystallize in the $P2_1/m$ space group. Topological analyses suggest that these frameworks possess the same two–dimensional (2D) (4,4)-connected networks. Notably, the emission spectrum reveals the fluorescence of complex **1** is mainly from the ligands to ligands charge transfer transition. Further investigation indicates that complex **1** can act as a fluorescent sensor for highly sensitive and selective detection of Fe^{3+} and 2,4,6-trinitrophenol (TNP) in MeCN solution, the quenching constants (K_{sv}) are 1.45×10^5 M^{-1} for Fe^{3+} and 4.08×10^4 M^{-1} for TNP, with the detection limit (LOD) of 0.12 μM for Fe^{3+} and 0.52 μM for TNP. Furthermore, the possible sensing mechanisms of complex **1** as bifunctional sensors have been studied based on experiments.

Graphical Abstract

Two isostructural rare earth metal–organic frameworks based on 1, 1'−butadiynebenzene−3, 3', 5, 5'−tetracarboxylate ligand were synthesized and structurally characterized in detail, and complex **1** is promising bifunctional luminescent probe for

---

highly sensitive and selective sensing Fe^{3+} ions and TNP through luminescence quenching effect, complex **1** also exhibits good recyclability for detecting Fe^{3+} ions and TNP. The quenching mechanisms were studied as well.
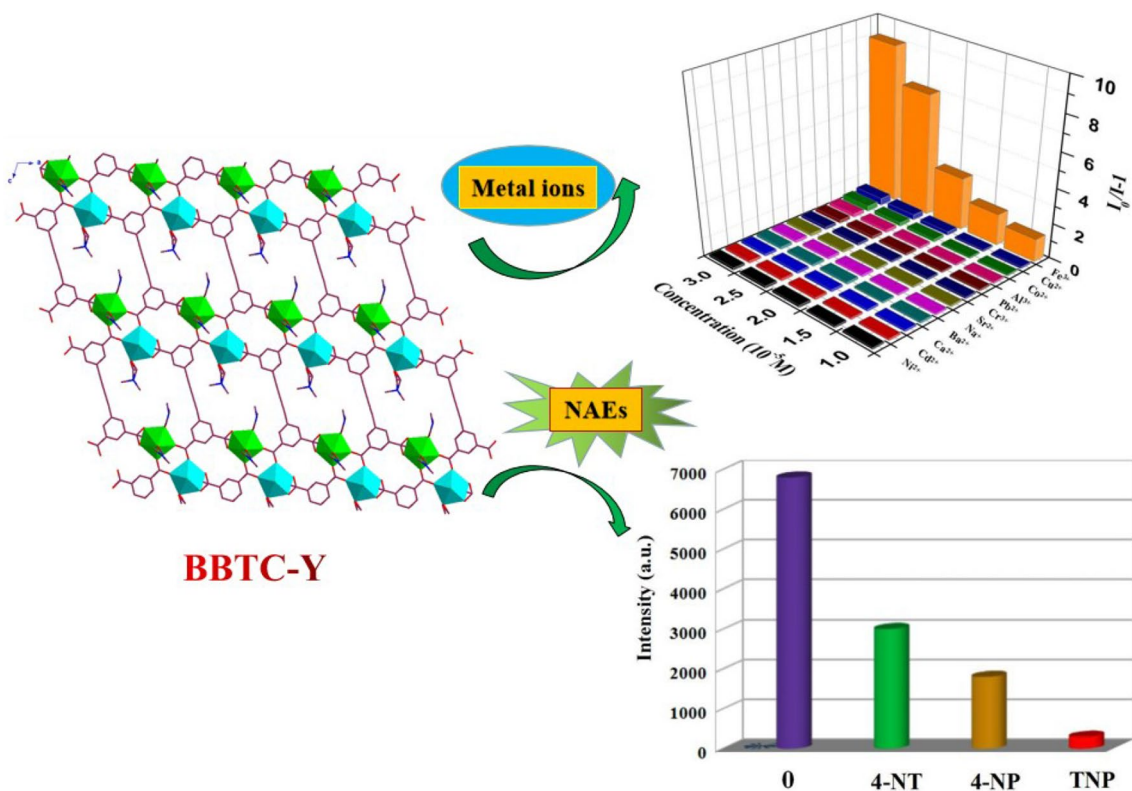
1 Introduction

With the vigorous development of chemical industry, the discharged pollutants produced by factories are increasing. Metal ions and nitro-aromatic explosives (NAEs) in the pollutants have aroused widespread concerns because of their threat to ecological environment and public security [1–3]. Many metal ions, especially to highly-charged metal ions, which could cause irreversible damage to living organisms and ecosystem if these metal ions are discharged into the environment, and the Fe^{3+} ion is also considered as toxic pollutant when the concentration is too high [4–6]. Nitro-aromatic explosives (NAEs) (trinitrophenol, p-nitrophenol, 4-nitrobenzene) are highly toxic chemicals, which exist in industrial production such as dyes, pharmaceuticals, explosives and paints, have irritating effects on eyes, respiratory tract and skin, and threaten people's life and health [7–10]. In addition, NAEs are

strong oxidants, which react violently with reducing agents to cause explosions, which are very harmful to society [11–14]. Therefore, the effective detection of NAEs is of great significance to people's production and life. At present, the traditional methods for detecting ions/molecules mainly include mass spectrometry, gas chromatography, high performance liquid chromatography, raman spectroscopy, ion mobility spectrometry and atomic absorption spectrometry. However, these traditional detection methods have the disadvantages of complicated operation, inconvenient equipment and high detection cost [15–17]. Therefore, it is very necessary to develop a fast, convenient, effective and cheap detection technology to detect metal ions and NAEs. These problems are still great challenges for scientific researchers.

In recent years, researchers have adopted some porous materials as sensors for detecting various metal ions and NAEs. Re-MOF (rare earth metal–organic framework) is a kind of porous skeleton material formed by

self-assembly of rare earth metal nodes (ions, chains or clusters) and organic ligands. This kind of material not only has high porosity, adjustable pores diameter, diverse topological structure, but also has unique luminescent advantages, such as high color purity, large stokes shift, high quantum yield, narrow emission band [18, 19]. Due to the advantages of high sensitivity, fast response and real-time monitoring, Re-MOFs have become more and more attractive in the field of detection, many Re-MOFs have been developed into luminescent sensors for various harmful pollutants in the environment [20–22].

Up to now, researchers have reported some Re-MOFs for fluorescence detection of metal ions and NAEs. Liu et al. reported a series of isomorphic Re-MOFs, which have high sensitivity and selectivity for Fe^{3+}, 2,4-DNP and 4-NP, respectively, and can be quickly detected and identified [23]. Wu et al. successfully constructed a multi-response fluorescence sensor (Ga-MOF), which can effectively detect Fe^{3+} and nitrobenzene with high selectivity and sensitivity [24]. Zhang et al. reported a series of Eu^{3+}/Tb^{3+}-MOFs, all of the compounds were developed as efficient fluorescence "turn-off" sensors to detect Fe^{3+} and 4-NP in DMF solutions [25]. The above results prompted us to continue to explore new luminescent Re-MOFs as candidate materials for multifunctional sensors.

On the other hand, the relatively soft tetracarboxylic acid ligand (1,1'-butadiynebenzene-3,3',5,5'-tetracarboxylate) (H$_4$BBTC) can make two aromatic rings rotate freely because of its butadiyne group. This feature is helpful to construct MOFs with novel topological structure and multifunctional properties. Some MOFs based on this ligand have shown good activity in gas adsorption and magnetic applications [26–28]. More importantly, in view of the large conjugated system of H$_4$BBTC ligand, it is expected that this ligand can be used to construct MOFs with good fluorescence activity. However, as far as we know, the application of MOFs based on H$_4$BBTC ligand in the fluorescence detection of Fe^{3+} and NAEs has not been reported so far.

Based on the above considerations, and in continuation to our previous investigations on construction of MOFs from butadiynebenzene–carboxylate ligand, two isostructural 2D Re-MOFs [Re = Y (**1**) and Ho (**2**)], were successfully synthesized through solvothermal method. Re-BBTC were assembled with dinuclear $Re_2(CO_2)_2$ SBU units and $BBTC^{4-}$ ligands, both structures were distinct from other known Cu(II) and Eu(III) MOFs with the same ligand [29, 30]. Notably, complex **1** exhibited high sensitivity and good selectivity towards Fe^{3+} and TNP, respectively. The fluorescence quenching may be attributed to the resonance energy transfer between analytes and skeletons.

2 Experimental

2.1 Materials and Measurements

1,1'-butadiynebenzene-3,3',5,5'-tetracarboxylate (H$_4$BBTC) was prepared according to the method in the previous literature [29, 30]. $YCl_3 \cdot 6H_2O$ and $HoCl_3 \cdot 6H_2O$ were purchased from chemical company and used directly. All reagents and materials are of analytical grade and used without further purification.

The measurement of powder X-ray diffraction (PXRD) was carried out at room temperature with Cu Kα ($\lambda = 1.54056$ Å) radiation at a scanning speed of 5° min^{-1} and a step size of 0.02° in 2θ. The elemental analysis (C, H and N) was performed on Perkin-Elmer 240 elemental analyzer, and the IR spectrum was measured with KBr pellets on a NICOLET iS10 spectrometer. Using DTA-TGA 2960 thermogravimetric analyzer, thermogravimetric analysis (TGA) was performed at a heating rate of 20 °C min^{-1} under N_2 atmosphere, and photoluminescence spectra were recorded at room temperature with Hitachi F4600 fluorescence spectrometer. UV–Vis spectra were collected on PerkinElmer Lambda 365 UV–Vis spectrophotometer.

2.2 Synthesis of Complexes 1 and 2

[Y$_2$(BBTC)(DMF)$_5$Cl$_2$]·2DMF·H$_2$O (1). A solution of H$_4$BBTC (5 mg, 0.013 mmol), $YCl_3 \cdot 6H_2O$ (8 mg, 0.026 mmol), DMF (0.4 mL) and HCl (0.03 mL, 1 M in DMF) were mixed and sealed in a 15 mL Teflon–lined autoclave and heated to 85 °C for 24 h. Colourless block–shaped crystals were obtained after gradually cooled to room temperature at a rate of 5 °C h^{-1} (yield: 65% based on Y). Anal. calcd for $C_{41}H_{57}Cl_2Y_2N_7O_{16}$: C, 42.74; H, 4.98; N, 8.51. Found: C, 42.82; H, 4.76; N, 8.71. Selected IR data (KBr pellet, cm^{-1}): 3269 (b), 3071 (w), 2933 (w), 1650 (s), 1554 (m), 1435 (s), 1379 (s), 1250 (m), 1110 (s), 779 (s), 735 (s), 716 (s).

The analogous procedure above–mentioned was used for preparation of complex **2** (see ESI†).

2.3 Crystal Structure Determination

X-ray analyses of single crystals were carried out on Bruker Smart Apex II CCD diffractometer using graphite monochromatic Mo/Kα radiation ($\lambda = 0.71073$ Å) at 296 K. Using SAINT and SADABS software packages for data reductions and absorption corrections [31]. By using the direct method of SHELXL − 97 software package [32], the structures were solved. All hydrogen atoms were placed at the calculated positions and refined on the parent atoms.

All non-hydrogen atoms were anisotropically refined by full−matrix least−squares method on F^2. In complexes **1** and **2**, solvent molecules in the structures were highly disordered, so it was impossible to refine them by using the traditional discrete–atom models. In order to solve this problem, the contribution of solvent electron density was removed by SQUEEZE routine in PLATON [33]. The main data of collection and refinement details of complexes **1** and **2** are given in Table 1. The selected bond lengths and bond angles are listed in Tables Sl and S2†. The CCDC reference numbers are 2,308,970 for complex **1** and 2,308,971 for complex **2**, respectively.

3 Results and Discussion

3.1 Crystal Structures

Single crystal X–ray diffraction analyses reveal that complexes **1** and **2** are isomorphous, exhibit similar 2D frameworks. Besides this, the IR spectra of complexes **1** and **2** are almost identical (Fig. S1†). As a result, only the structure of

Table 1 Crystallographic data and structural refinements for **1** and **2**

Complex	1	2
Empirical formula	$C_{41}H_{57}Cl_2Y_2N_7O_{16}$	$C_{41}H_{57}Cl_2Ho_2N_7O_{16}$
Formula weight	1152.65	1304.70
Crystal system	Monoclinic	Monoclinic
Space group	$P2_1/m$	$P2_1/m$
a (Å)	10.88(1)	10.95(1)
b (Å)	16.07(1)	16.28(1)
c (Å)	16.36(1)	16.44(1)
α (°)	90.00	90.00
β (°)	105.27(1)	105.35(2)
γ (°)	90.00	90.00
V (Å^3)	2760.2(4)	2825(4)
Z	2	2
D_c (g·cm^{-3})	1.365	1.512
μ (mm^{-1})	2.252	2.937
$F(000)$	1164	1276
Reflection collected	7097	6513
Unique reflection	4348	5766
R_{int}	0.0597	0.0351
Completeness (%)	99.3	99.0
θ rang for data collection (°)	1.81~28.36	2.2996~27.2782
GOF	1.082	1.085
$R_1{}^a$, $wR_2{}^b$ [$I > 2\sigma(I)$]	0.1257, 0.2637	0.0835, 0.2323
$R_1{}^a$, $wR_2{}^b$ (all data)	0.1784, 0.2887	0.0916, 0.2401

$^aR_1 = \Sigma||F_o| - |F_c||/\Sigma|F_o|$

$^bwR_2 = \{\Sigma[w(F_o{}^2 - F_c{}^2)^2]/\Sigma(w(F_o{}^2)^2)]\}^{1/2}$

$[Y_2(BBTC)(DMF)_5Cl_2]\cdot2DMF\cdot H_2O$ (**1**) is representatively described in detail. The structure of complex **2** is shown in Fig. S2†.

Crystal **1** belongs to monoclinic system, and its space group is $P2_1/m$. As shown in Fig. 1a, its asymmetric unit cell contains one eight−coordinated Y^{3+} ion (denoted as Y1), one seven−coordinated Y^{3+} ion (denoted as Y2), one completely deprotonated BBTC^{4-} ligand, five coordinated DMF molecules and two coordinated Cl$^-$ ions. Two crystallographically independent Y^{3+} ions show two different coordination geometries (Fig. 1b). The coordination geometry around Y1 ion can be described as a distorted dodecahedron, and its eight coordination oxygen atoms come from three BBTC^{4-} ligands (O2, O3c, O4c and O8a) and four DMF molecules (O9, O9b, O10 and O10b). For Y2 ions, they are bonded with four oxygen (O1, O7a, O5d and O6d) from three BBTC^{4-} ligands, the other oxygen (O12) from one DMF molecule and two Cl$^-$ ions (labeled Cl1 and Cl1b respectively), resulting in a distorted pentagonal bipyramid geometry. Among the four coordinated BBTC^{4-} ligands, two carboxylate groups from two BBTC^{4-} ligands coordinate with Y1 and Y2 centers in a chelating manner, while the other two carboxylate groups from two different BBTC^{4-} ligands coordinate with Y1 and Y2 centers in a bidentate bridging manner, resulting in a binuclear $Y_2(CO_2)_2$ subunit (SBU), in which the Y1···Y2 distance is 5.589 Å (Fig. 1c). The torsion angle of the diacetylene group (C9−C10−C11−C12) is 0.994°, and the dihedral angle between two benzene rings is 0°. These data show that BBTC^{4-} is nearly symmetrical, and the two benzene rings of BBTC^{4-} are basically coplanar to meet the coordination geometry of Y^{3+}. The Y−O bond lengths range from 2.227(7) to 2.397(6) Å (Table S1†), and the O−Y−O bond angles range from 51.8(2) to 161.0(2)° (Table S2†). These bond parameters are similar to the values of Re-carboxylate complexes in references [34, 35].

The carboxylate groups in complex **1** are coordinated with two Y^{3+} ions by chelating and bidentate bridging to form a binuclear Y cluster unit $Y_2(CO_2)_2$ SBU. Generally speaking, each $Y_2(CO_2)_2$ SBU is surrounded by four BBTC^{4-} ligands, and each BBTC^{4-} ligand connects four $Y_2(CO_2)_2$ SBUs, resulting in a two-dimensional (2D) network framework (Fig. 1d and e). From the topological point of view, each $Y_2(CO_2)_2$ SBU is regarded as a 4−connected node and the organic ligand BBTC^{4-} is considered as a 4−connected node, the 2D structure of complex **1** can be described as a (4,4)−connected network (Fig. 1f).

3.2 Powder X-Ray Diffraction (PXRD) and Thermal Stability

Powder X–ray diffraction (PXRD) of complexes **1** and **2** were recorded at room temperature. As shown in Fig. S3†, the curves of the two complexes are similar, revealing that
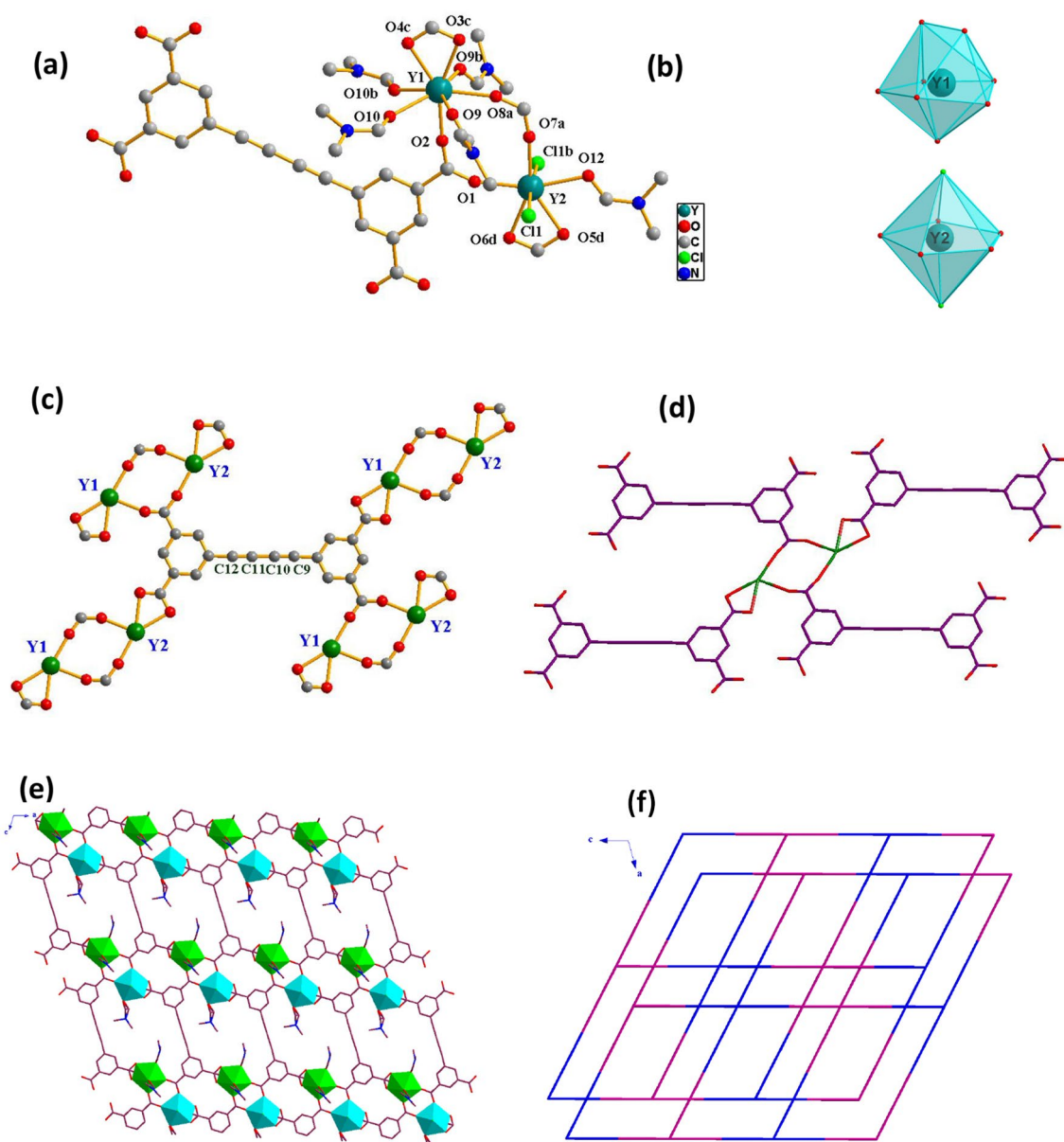
Fig. 1 (**a**) Coordination environments of Y^{3+} ions with the H atoms omitted for clarity; Symmetry codes: a=x, y, 1+z; b=x, 1.5−y, z; c=−1+x, y, z; d=1+x, y, 1+z; **b** Coordination polyhedron of Y^{3+} ions; **c** One BBTC^{4-} ligand links four $Y_2(CO_2)_2$ SBUs; **d** One $Y_2(CO_2)_2$ SBU is connected by four BBTC^{4-} ligands; **e** Polyhedral representation of complex **1** seen from *b* direction (the green and turquoise polyhedra correspond to [Y1O$_8$] and [Y2O$_5$Cl$_2$]units, respectively; **f** (4,4)-connected network presented, red represents the 4-connected node of organic ligand and blue represents the 4-connected node of U in complex **1** seen from *b* direction

complexes **1** and **2** are isostructural with each other. The peak positions of the theoretical and experimental PXRD patterns are in good agreement with each other, which clearly indicate the high purity of these samples.

TGA measurements of complexes **1** and **2** were performed from room temperature to 700 °C under a nitrogen atmosphere (Fig. S4†), the isomorphism complexes **1** and **2** exhibit similar thermal behavior with several sequential weight loss processes. Considering the isomorphism of complexes **1** and **2**, complex **1** is discussed as the representative example in detail. As shown in Fig. S4a†, Complex **1** shows sequential weight loss process with a percentage of 14.67% before 90 °C, corresponding to the loss of one guest H_2O molecule and two guest DMF molecules per formula unit (calcd: 14.23%), and the second weight loss of 31.34% in 91−335 °C temperature range, attributing to the release of five coordinated DMF molecules per formula unit (calcd: 31.66%). Above 335 °C, the whole framework gradually begins to break down upon further heating.

3.3 Fluorescent Behavior

The solid−state luminescence properties of H_4BBTC and complex **1** were investigated at room temperature. As shown in Fig. S5†, it is observed that H_4BBTC exhibits a broad emission centered at 420 nm upon excitation at 340 nm due to the charge transfer in the organic ligand ($\pi^* \rightarrow \pi$) [36]. The electronic structure of Y^{3+} ion is a closed shell with no f–f transition, so it is a non-luminous rare earth ion. Therefore, at the same excitation wavelength, complex **1** displays luminescence with a single broad emission band centered at 402 nm, such a broad band emission of complex **1** can also be assigned to the ligand to ligand charge transfer of carboxylic acids [37]. In comparison to the emission of H_4BBTC, the blue shift of the emission band (18 nm) may be attributed to the energy transfer from the ligand to the Y^{3+} ion [38–40].

The emission of complex **2** in the near–IR region was also investigated, which is a rarely described phenomenon [41, 42]. Three emission bands centered at 989 ($^5F_5 \rightarrow {}^5I_7$), 1177 ($^5F_6 \rightarrow {}^5I_8$) and 1478 nm ($^5F_5 \rightarrow {}^5I_6$) are observed for the Ho^{3+} complex (Fig. S6†).

In order to explore the luminescence properties of complex **1** in various organic solvents, emission spectra of complex **1** suspended in different solvents were studied. The details are as follows: the finely ground samples of complex **1** (2 mg) were dispersed into different solvents (2.0 mL), such as acetonitrile (MeCN), ethyl acetate, chloroform ($CHCl_3$), dichloromethane (DCM), N, N-dimethylformamide (DMF), tetrahydrofuran (THF), benzene, toluene and acetone to form stable suspensions. As shown in Fig. 2, the emission intensities of complex **1** were dependent on the solvent molecules, and the results showed that complex **1** displayed the strongest luminescence emission intensity in MeCN solution. Undoubtedly, MeCN was selected as the solvent to carry out a series of luminescence sensing experiments.
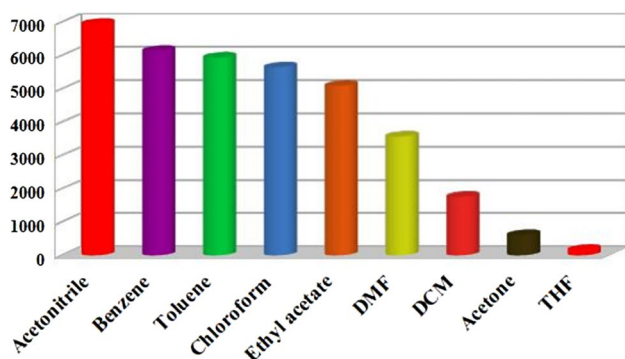

Fig. 2 Comparisons of the luminescence intensity of complex **1** in different solvents at room temperature

3.4 Fluorescence Sensing Properties

3.4.1 Sensing of Cations

First, complex **1** (2 mg) was dispersed in the solution of $M(NO_3)_x$ (2 mL) (M^{x+} = Fe^{3+}, Cu^{2+}, Cr^{3+}, Pb^{2+}, Al^{3+}, Ni^{2+}, Co^{2+}, Ca^{2+}, Cd^{2+}, Sr^{2+}, Ba^{2+}, Na^+; 1×10^{-2} mol L^{-1}). Then the fluorescence intensities of suspensions containing above 12 kinds of metal ions were recorded and compared, respectively. It can be clearly seen that among the all detected metal ions, the luminescence quenching ability of complex **1** to Fe^{3+} was the strongest, with a quenching efficiency of 90.26% for complex **1** (Fig. 3a). To further study, the luminescence titration experiments were performed by incremental addition of Fe^{3+} (1 mM) to the suspension of complex **1**. It can be seen from Fig. 3b and c that the fluorescence intensity of complex **1** decreased gradually with the increasing concentration of Fe^{3+}, and the fluorescence intensity of complex **1** was quenched to over 90% when the amount of Fe^{3+} ions was added to 60 μL. The quenching effect of Fe^{3+} ions on complex **1** can be explained quantitatively by the Stern–Volmer (SV) equation: $(I_0/I) = 1 + K_{sv}[C]$. In the equation, I_0 and I are the intensities of complex **1** before and after addition of Fe^{3+}, [C] is the concentration of Fe^{3+} and K_{sv} is the quenching constant [43]. The Sterm-Volmer plot for Fe^{3+} is nearly linear at low concentrations and subsequently deviated from linearity, bending upwards at higher concentrations (Fig. 3d). The nonlinear nature of the SV plot can be ascribed to a self-absorption or energy transfer process [44–46].

According to the equation calculation, the quenching constant of Fe^{3+} ion on complex **1** is calculated to be 1.45×10^5 M^{-1}, which is larger than most of the reported MOF-based Fe^{3+} sensors, and the limit of detection (LOD) is calculated to be 0.12 μM, which is relatively low in comparison to that in the reported examples (Table S3†), indicating that at very low concentrations, complex **1** still has a significant fluorescence response to Fe^{3+}, which shows that complex **1** has good detection sensitivity for Fe^{3+} [47]. To examine the sensing selectivity of complex **1** towards Fe^{3+} ions, the anti-interference experiments were carried out, and the results showed that the quenching efficiency of complex **1** toward Fe^{3+} was hardly affected by other interfering metal ions, indicating that Fe^{3+} had good anti-interference capability (Fig. 4a) [48]. Additionally, others fluorescence titration experiments were performed by adding other metal ions as well, as shown in Fig. 4b, the selectivity of complex **1** for Fe^{3+} was found to be very high by comparison with other ions [49].
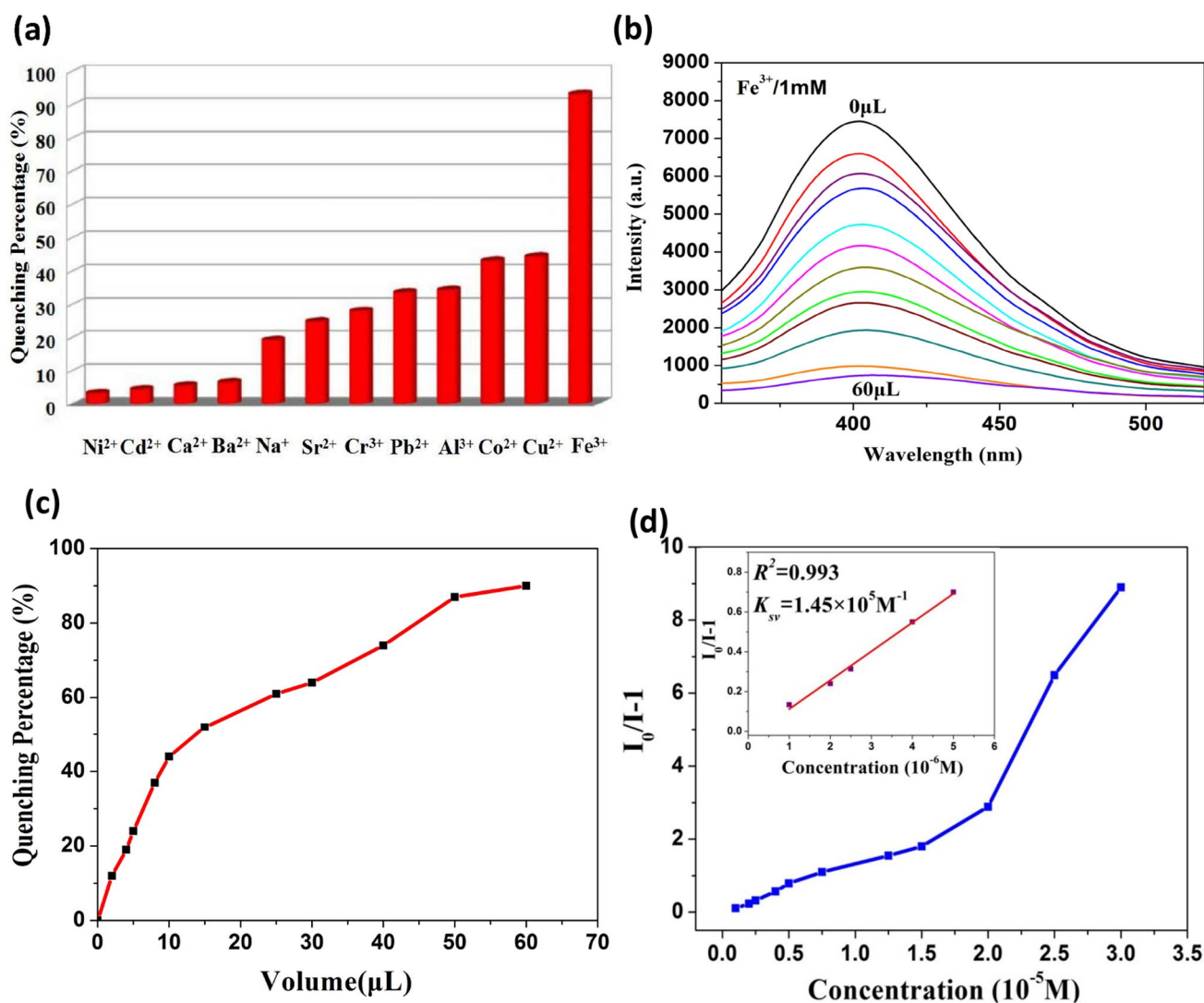
(a)

(b)

(c)

(d)

Fig. 3 **a** Luminescence quenching efficiency of complex **1** in various metal ions (1×10^{-2} mol L^{-1}); **b** Emission spectra of complex **1** dispersed in MeCN after addition of Fe^{3+} solution (1 mM); **c** Quenching percentages of complex **1** upon addition of different volumes of 1 mM Fe^{3+} solution; **d** Stern–Volmer plots of complex **1** dispersed in MeCN at different concentrations of Fe^{3+} ions, the insert plot shows the correlation between the concentration of Fe^{3+} and $(I_0 - I)/I$

3.4.2 Sensing of NAEs

Similar to the fluorescence detection of metal ions, NAEs (4-nitrophenol (4-NP), 2,4,6-trinitrophenol (TNP) and 4-nitrotoluene (4-NT)) with a concentration of 5×10^{-3} moL L^{-1} were selected for sensing experiments. As shown in Fig. S7†, all the NAEs have a certain fluorescence weakening effect on complex **1**, while TNP have excellent luminescent quenching efficiency, the quench order is as follows: TNP > 4-NP > 4-NT. This result indicate that complex **1** possesses a highly selectivity for sensing TNP compared to other nitro-aromatic explosives [50].

For further study the luminescent quenching efficiency, the titration experiments were performed to explore the

sensitivity of complex **1** to three different NAEs, respectively. It was found that the fluorescence intensity of complex **1** gradually weakened with the increasing of NAEs concentrations, and the fluorescence quenching process can be observed in Fig. 5 and S8–S9†. Interestingly, the quenching efficiency can be as high as 94% after adding 100 μL TNP solution (Fig. 5a and b). In the low concentration range of NAEs, the calculated K_{sv} of complex **1** for the above three NAEs are shown in Table S4†, the quenching constant of complex **1** for TNP is calculated to be 4.08×10^4 M^{-1} (Fig. 5c), which is equivalent to some recent reports of MOF-based TNP sensors, and the LOD value for TNP is calculated to be 0.52 μM, which is comparable to most of reported MOF-based sensors (Table S5†). The LOD of TNP
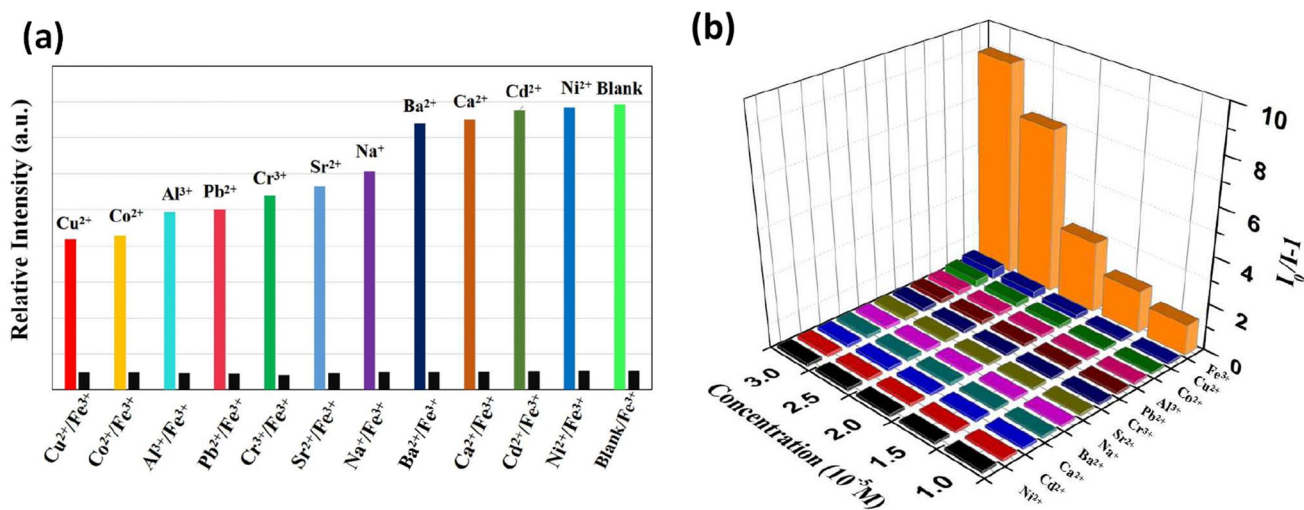
Fig. 4 **a** Luminescence intensities of complex **1** in different metal ions (1×10^{-2} mol L^{-1}) and mixed-metal solutions containing Fe^{3+} (1×10^{-2} mol L^{-1}); **b** Stern–Volmer plot of I_0/I-1 versus different metal ions concentration in MeCN

is small, indicating that complex **1** has high sensitivity for detecting TNP [51].

3.5 Recyclability and Stability of Complex 1

Further more, the recyclability experiments of complex **1** in sensing Fe^{3+} and NAEs processing were further explored, the suspensions of complex **1** were centrifuged and washed with CH$_3$CN after every titration measurement cycle. As depicted in Fig. 6 and S10–S11†, it was found that complex **1** can still maintain good luminescence intensity and the quenching ability after being used for four times. The PXRD patterns reveal the positions and intensities of complex **1** have not significantly changed after four quenching recovery cycles, showing the good recyclability and high stability of complex **1** (Fig. S12†) [49].

3.6 Fluorescence Quenching Mechanism of Complex 1

The fluorescent response rates of complex **1** to Fe^{3+} and TNP at different immersing time intervals show that the fluorescence intensity can reach the least values quickly within one minute (Fig. S13 and S14†), which can be deduced that the fluorescence quenching mechanism is not caused by the adsorption of Fe^{3+} or TNP in complex **1** [52]. In addition, the ultraviolet–visible absorption spectra of metal ions in MeCN solution (5×10^{-4} mol L^{-1}) were measured, respectively. As shown in Fig. S15†, the absorption spectrum of

Fe^{3+} overlaps with the emission spectrum of complex **1** to a certain extent, but there is less overlap with other metal ions. It means that Fe^{3+} can effectively absorb the energy of the emitted light of complex **1**, and the luminescence quenching mechanism is mainly energy resonance transfer [53–55]. Subsequently, the ultraviolet–visible absorption spectra of NAEs (1×10^{-4} mol L^{-1}) in MeCN solution were also tested. The results are shown in Fig. S16†, the ultraviolet absorption spectra of the three NAEs overlap with the emission spectra of complex **1** to a certain extent, but the spectral line of TNP overlap the most, indicating that the luminescence quenching of complex **1** is due to the NAEs effectively absorbing the energy of the emitted light of complex **1**, and the quenching mechanism is mainly energy resonance transfer [56, 57].

4 Conclusions

In summary, two isomorphic rare earth MOFs (Re-BBTC) with 2D layers composed of binuclear secondary building units and BBTC^{4-} were successfully synthesized under solvothermal conditions. Fluorescence experiments showed that Y-BBTC had efficient response in detecting Fe^{3+} and TNP with good sensitivity and selectivity. Combined with UV–Vis experimental results, the fluorescence quenching may be attributed to the resonance energy transfer between the analytes and the skeletons.
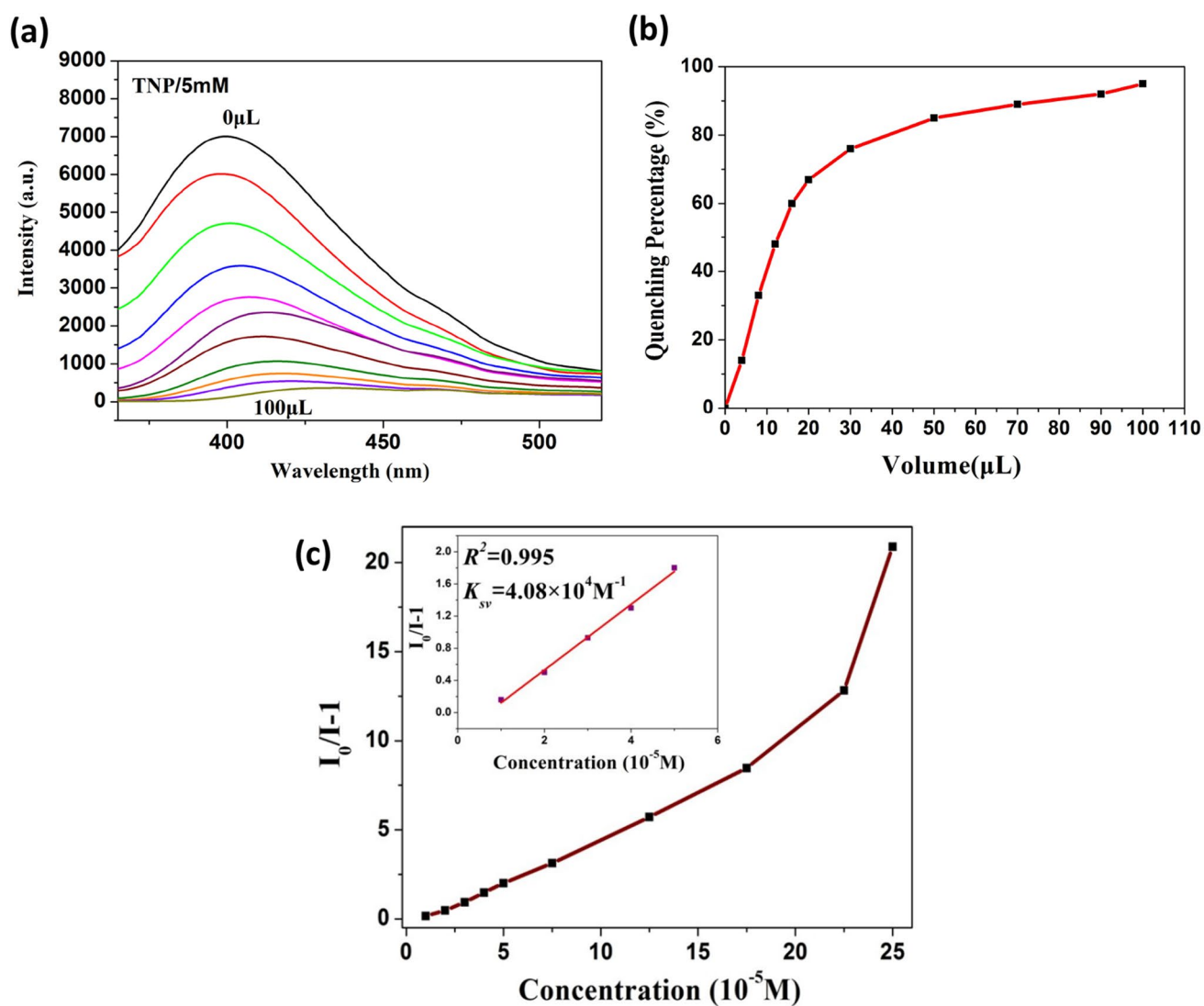
Fig. 5 **a** The changes of emission spectra upon incremental addition of TNP solution (5 mM); **b** Quenching percentages of complex **1** upon addition of different volumes of 5 mM TNP solution; **c** S–V plot of complex **1** upon incremental addition of TNP solution (5 mM) in MeCN
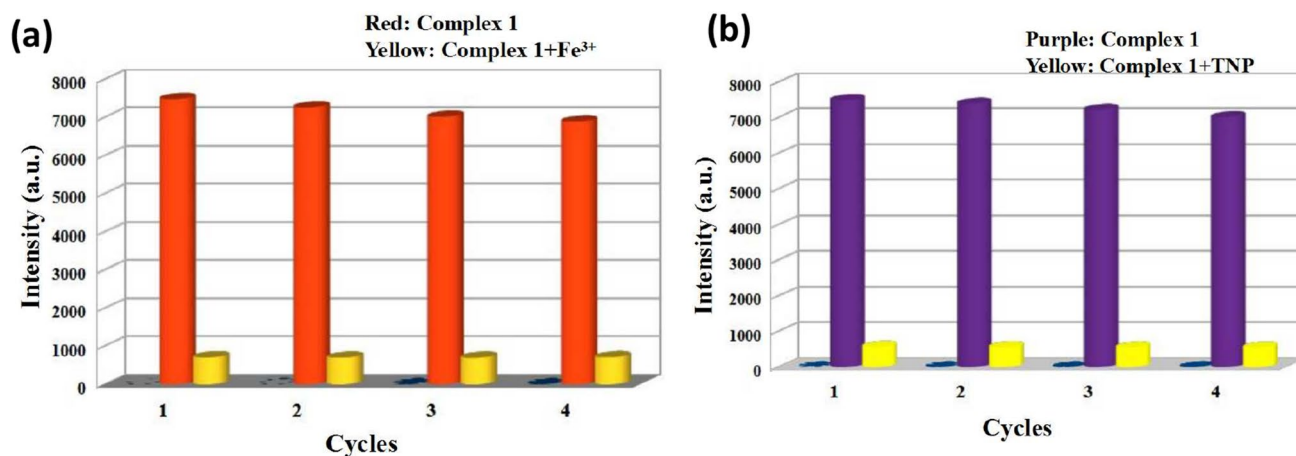

Fig. 6 The emission intensities of complex **1** for detecting Fe^{3+} (**a**) and TNP (**b**) in four fluorescence quenching-recovery cycles

Declarations

Competing interest The authors declare that they have no known competing financial interests or personal relationships that could have appeared to influence the work reported in this paper.

Supporting Information CCDC 2308970 for **1** and 2308971 for **2** contains the supplementary crystallographic data. These data can be obtained free of charge via http://www.ccdc.cam.ac.uk/conts/retrieving.html, or from the Cambridge Crystallographic Data Centre, 12 Union Road, Cambridge CB2 1EZ, UK; fax: (+44) 1223–336-033; or email: deposit@ ccdc.cam.ac.uk.

References

1. W.H. Yao, X.G. Mu, C.Y. He, Y.H. Zhang, Metal organic frameworks based on mixed ligands: syntheses, structures and selective detection of nitro explosive TNP, metal ions Fe^{3+} Cu^{2+} and CrO_4^{2-}. J. Mol. Struct. **1289**, 135886 (2023)

2. V.J. Mollá, C.M. Mezquita, C.G. Saiz, F.M. Romero, Zinc(II) picolinate-based coordination polymers as luminescent sensors of Fe^{3+} ions and nitroaromatic compounds. Inorg. Chim. Acta **538**, 120993 (2022)

3. B. Li, R. Li, J. Gao, W. Wang, J. Lu, F. Zheng, G. Guo, Barium-based coordination polymer: a bi-functional fluorescent sensor for Fe^{3+} and nitroaromatic molecular detection. Inorg. Chem. Commun. **137**, 109227 (2022)

4. Y. Liu, C.H. Sun, D. Yuan, L.W. Zhu, A fluorescent test paper fabricated by in situ growth of a functional Zn-MOF for fast and effective detection of Cr(VI) and Fe(III). Inorg. Chem. Commun. **146**, 110211 (2022)

5. Y. Yu, Y. Wang, H. Yan, J. Lu, H. Liu, Y. Li, S. Wang, D. Li, J. Dou, L. Yang, Z. Zhou, Multiresponsive luminescent sensitivities of a 3D Cd-CP with visual turn-on and ratiometric sensing toward Al^{3+} and Cr^{3+} as well as turn-off sensing toward Fe^{3+}. Inorg. Chem. **59**, 3828–3837 (2020)

6. Q.Y. Li, X.J. Wu, X.L. Huang, Y.J. Deng, N.J. Chen, D.D. Jiang, L.L. Zhao, Z.H. Lin, Y.G. Zhao, Tailoring the fluorescence of AIE-active metal–organic frameworks for aqueous sensing of metal ions. ACS Appl. Mater. Interfaces **10**, 3801–3809 (2018)

7. H.Z. Li, Q.M. Chen, Z.X. Zhang, Z.L. Wang, Z.J. Gong, M.K. Fan, Functionalized fluorescent Zr-MOF based on photoinduced electron transfer for highly sensitive detection of nitroaromatic explosives. Dyes. Pigments. **210**, 111035 (2023)

8. B. Dey, P. Pahari, S.K. Sahoo, A.K. Atta, Triazole-based pyrene-sugar analogues for selective detection of picric acid in water medium and paper strips. J. Photochem. Photobiol. A **440**, 114647 (2023)

9. B. Jiang, W. Liu, S. Liu, W.S. Liu, Coumarin-encapsulated MOF luminescence sensor for detection of picric acid in water environment. Dyes. Pigments. **184**, 108794 (2021)

10. Y. Nailwal, M. Devi, S.K. Pal, Luminescent conjugated microporous polymers for selective sensing and ultrafast detection of picric acid. ACS Appl. Polym. Mater. **4**, 2648–2655 (2022)

11. M. Kaur, M. Yusuf, Y.F. Tsang, K.H. Kim, A.K. Malik, Amine/hydrazone functionalized Cd(II)/Zn(II) metal-organic framework for ultrafast sensitive detection of hazardous 2,4,6-trinitrophenol in water. Sci. Total. Environ. **857**, 159385 (2023)

12. M.S. Thippeswamy, L. Naik, C.V. Maridevarmath, H.M. Savanur, G.H. Malimath, Studies on the characterisation of thiophene substituted 1, 3, 4-oxadiazole derivative for the highly selective and sensitive detection of picric acid. J. Mol. Struct. **1264**, 133274 (2022)

13. S. Halder, P. Ghosh, A. Hazra, P. Banerjee, P. Roy, A quinoline-based compound for explosive 2,4,6-trinitrophenol sensing: experimental and DFT-D3 studies. New J. Chem. **42**, 8408–8414 (2018)

14. D.K. Dang, C. Sundaram, Y.L.T. Ngo, W.M. Choi, J.S. Chung, E.J. Kim, S.H. Hur, Pyromellitic acid-derived highly fluorescent N-doped carbon dots for the sensitive and selective determination of 4-nitrophenol. Dyes. Pigments. **165**, 327–334 (2019)

15. M. McCullagh, K. Giles, K. Richardson, S. Stead, M. Palmer, Investigations into the performance of travelling wave enabled conventional and cyclic ion mobility systems to characterise protomers of fluoroquinolone antibiotic residues. Rapid Commun. Mass Spectrom. **33**, 11–21 (2019)

16. H.M. He, S.H. Chen, D.Y. Zhang, E.C. Yang, X.J. Zhao, A luminescent metal–organic framework as an ideal chemosensor for nitroaromatic compounds. RSC Adv. **7**, 38871–38876 (2017)

17. J.J. Qian, L.G. Qiu, Y.M. Wang, Y.P. Yuan, A.J. Xie, Y.H. Shen, Fabrication of magnetically separable fluorescent terbium-based MOF nanospheres for highly selective trace-level detection of TNT. Dalton Trans. **43**, 3978–3983 (2014)

18. X.Z. Song, Y.X. Wang, J.W. Yan, X. Chen, Y.L. Meng, Z. Tan, Enhancing the Fe^{3+} sensing sensitivity by energy transfer and phase transformation in a bimetallic lanthanide metal-organic framework. ChemistrySelect **3**, 9564–9570 (2018)

19. L. Feng, C. Dong, M. Li, L. Li, X. Jiang, R. Gao, R. Wang, L. Zhang, Z. Ning, D. Gao, J. Bi, Terbium-based metal-organic frameworks: highly selective and fast respond sensor for styrene detection and construction of molecular logic gate. J. Hazard. Mater. **388**, 121816 (2020)

20. S.J. Wang, Q. Li, G.L. Xiu, L.X. You, F. Ding, R.V. Deun, I. Dragutan, V. Dragutan, Y.G. Sun, New Ln-MOFs based on mixed organic ligands: synthesis, structure and efficient luminescence sensing of the Hg^{2+} ions in aqueous solutions. Dalton Trans. **50**, 15612–15619 (2021)

21. B. Li, J.P. Dong, Z. Zhou, R. Wang, L.Y. Wang, S.Q. Zang, Robust lanthanide metal–organic frameworks with "all-in-one" multifunction: efficient gas adsorption and separation, tunable light emission and luminescence sensing. J. Mater. Chem. C. **9**, 3429–3439 (2021)

22. Y. Liu, J. Ma, C. Xu, Y. Yang, M. Xia, H. Jiang, W. Liu, A water-stable lanthanide coordination polymer as a multiresponsive luminescent sensor for Fe^{3+}, Cr(VI) and 4-nitrophenol. Dalton Trans. **47**, 13543–13549 (2018)

23. Q.L. Hu, T. Xu, J.M. Gu, L.R. Zhang, Y.L. Liu, A series of isostructural lanthanide metal–organic frameworks: effective fluorescence sensing for Fe^{3+}, 2,4-DNP and 4-NP. CrystEngComm **24**, 2759–2766 (2022)

24. J. Wu, H. Zhang, Y.H. Luo, W.Y. Geng, Y.Q. Lan, A microporous cationic Ga(III)-MOF with fluorescence properties for selective sensing Fe^{3+} ion and nitroaromatic compounds. Chem. J. Chinese Universities. **43**, 20210617 (2022)

25. X.F. Cheng, J.S. Hu, J.X. Li, M.D. Zhang, Tunable emission and selective luminescence sensing for nitro-pollutants and metal ions based on bifunctional lanthanide metal-organic frameworks. J. Lumin. **221**, 117100 (2020)

26. D. Zhao, D. Yuan, A. Yakovenko, H.C. Zhou, A NbO-type metal–organic framework derived from a polyyne-coupled di-isophthalate linker formed in situ. Chem. Commun. **46**, 4196–4198 (2010)

27. B. Zheng, Z.Q. Liang, G.H. Li, Q.S. Huo, Y.L. Liu, Synthesis, structure, and gas sorption studies of a three-dimensional metal−organic framework with NbO topology. Cryst. Growth Des. **10**, 3405–3409 (2010)

28. L.F. Wang, L.C. Kang, W.W. Zhang, F.M. Wang, X.M. Ren, Q.J. Meng, New europium coordination polymers with efficient energy transfer from conjugated tetracarboxylate ligands to Eu^{3+} ion: syntheses, structures, luminescence and magnetic properties. Dalton Trans. **40**, 9490–9497 (2011)

29. L.F. Wang, L. Zhai, X.M. Ren, W.W. Zhang, A microporous metal–organic framework with butynelene functionality for selective gas sorption. J. Solid State Chem. **204**, 53–58 (2013)

30. J.W. Rong, W.W. Zhang, J.F. Bai, Synthesis and structure of color tunable and white-light emitting lanthanide metal–organic framework materials constructed from conjugated 1,1′-butadiynebenzene-3,3′,5,5′-tetracarboxylate ligand. RSC Adv. **6**, 103714–103723 (2016)

31. Software packages SMART and SAINT, Siemens Analytical X-ray Instrument Inc., Madison, WI, 1996.

32. G.M. Sheldrick, *SHELX−97, Program for the refinement of crystal structure* (University of Göttingen, Germany, 1997)

33. A.L. Spek, J. Appl. Crystallogr. **36**, 7 (2003)

34. L.L. Luo, X.L. Qu, Z. Li, X. Li, H.L. Sun, Isostructural lanthanide-based metal–organic frameworks: structure, photoluminescence and magnetic properties. Dalton Trans. **47**, 925–934 (2018)

35. X.L. Lv, L. Feng, K.Y. Wang, L.H. Xie, T. He, W. Wu, J.R. Li, H.C. Zhou, A series of mesoporous rare-earth metal–organic frameworks constructed from organic secondary building units. Angew. Chem. Int. Ed. **60**, 2053–2057 (2021)

36. H. Liu, Y. Liu, Y. Meng, X. Shi, J. Sun, L. Zhao, D. Chen, H. Hao, D. Li, J. Dou, J. Han, Di-functional luminescent sensors based on Y^{3+} doped Eu^{3+} and Tb^{3+} coordination polymers: fast response and visible detection of Cr^{3+}, Fe^{3+} ions in aqueous solutions and acetone. RSC Adv. **10**, 32232–32240 (2020)

37. J.J. Liu, G.F. Ji, J.N. Xiao, Z.L. Liu, Ultrastable 1D europium complex for simultaneous and quantitative sensing of Cr(III) and Cr(VI) ions in aqueous solution with high selectivity and sensitivity. Inorg. Chem. **56**, 4197–4205 (2017)

38. Y.Q. Su, R.T. Wang, O.A. Blatova, Y.S. Shi, G.H. Cui, Two robust Zn(II)-organic frameworks as dual-functional fluorescent probes for efficient sensing of enrofloxacin and MnO_4^- anions. CrystEngComm **24**, 182–191 (2022)

39. J. Troyano, E. Zapata, J. Perles, P. Amo-Ochoa, V. Fernandez-Moreira, J.I. Martinez, F. Zamora, S. Delgado, Multifunctional copper(I) coordination polymers with aromatic mono- and ditopic thioamides. Inorg. Chem. **58**, 3290–3301 (2019)

40. X. Zhou, Y.X. Shi, C. Cao, C.Y. Ni, Z.G. Ren, D.J. Young, J.P. Lang, Nickel(II)-based two-dimensional coordination polymer displaying superior capabilities for selective sensing of Cr(VI) ions in water. Cryst. Growth Des. **19**, 3518–3528 (2019)

41. K. Driesen, R. Van Deun, C. Görller-Walrand, K. Binnemans, Near-infrared luminescence of lanthanide calcein and lanthanide dipicolinate complexes doped into a silica−PEG hybrid material. Chem. Mater. **16**, 1531–1535 (2004)

42. K. Lunstroot, P. Nockemann, K. Van Hecke, L. Van Meervelt, C. Görller-Walrand, K. Binnemans, K. Driesen, Visible and near-infrared emission by samarium(III)-containing ionic liquid mixtures. Inorg. Chem. **48**, 3018–3026 (2009)

43. A. Buragohain, M. Yousufuddin, M. Sarma, S. Biswas, 3D luminescent amide-functionalized cadmium tetrazolate framework for selective detection of 2,4,6-trinitrophenol. Cryst. Growth Des. **16**, 842–851 (2016)

44. S.S. Nagarkar, B. Joarder, A.K. Chaudhari, S. Mukherjee, S.K. Ghosh, Highly selective detection of nitro explosives by a luminescent metal–organic framework. Angew. Chem. Int. Ed. **125**, 2953–3957 (2013)

45. X.H. Zhou, L. Li, H.H. Li, A. Li, T. Yang, W. Huang, A flexible Eu(III)-based metal–organic framework: turn-off luminescent sensor for the detection of Fe(III) and picric acid. Dalton Trans. **42**, 12403–12409 (2013)

46. S.R. Zhang, D.Y. Du, J.S. Qin, S.L. Li, W.W. He, Y.Q. Lan, Z.M. Su, 2D Cd(II)–lanthanide(III) heterometallic–organic frameworks based on metalloligands for tunable luminescence and highly selective, sensitive, and recyclable detection of nitrobenzene. Inorg. Chem. **53**, 8105–8113 (2014)

47. K. Wu, J.S. Hu, S.N. Shi, J.X. Li, X.F. Cheng, A thermal stable pincer-MOF with high selective and sensitive nitro explosive TNP, metal ion Fe^{3+} and pH sensing in aqueous solution. Dyes. Pigments. **173**, 107993 (2020)

48. S.J. Dong, J.S. Hu, X.L. Zhang, M.D. Zheng, A bifunctional Zn(II)-MOF as recyclable luminescent sensor for detecting TNT and Fe^{3+} with high selectivity and sensitivity. Inorg. Chem. Commun. **97**, 180–186 (2018)

49. X.L. Zhang, J.S. Hu, B. Wang, Z.Q. Li, S.B. Xu, Y.N. Chen, X.M. Ma, A chiral zinc(II) metal-organic framework as high selective luminescent sensor for detecting trace nitro explosives picric acid and Fe^{3+} ion. J. Solid State Chem. **269**, 459–464 (2019)

50. J.X. Li, K.A. Nartey, X.J. Cao, M.D. Zhang, J.S. Hu, PH stable cationic luminescence metal−organic framework material with nitrate guests as high selective sensor for detecting 2,4,6-trinitrophenol. J. Solid State Chem. **290**, 121583 (2020)

51. X.L. Zhang, J.S. Hu, J.S. Li, T.T. Liu, J. Wang, X.M. Ma, A bifunctional luminescent coordination polymer as recyclable sensor for detecting TNP and Fe^{3+} with high selectivity and sensitivity. Inorg. Chim. Acta **486**, 556–561 (2019)

52. D.F. Liu, Q.Y. Zhu, G.L. Wen, W.W. Zhou, X.L. Wang, X. Liang, J.W. Rong, J.T. Shao, Assembly of a Cd(II)-organic framework based on 1,3,5-Tri(1H-imidazol-1-yl)benzene: synthesis, crystal structure, and luminescent sensing property. Inorg. Chim. Acta **512**, 119891 (2020)

53. Y.S. Shi, Y.H. Li, G.H. Cui, G.Y. Dong, New two-dimensional Cd(II) coordination networks bearing benzimidazolyl-based linkers as bifunctional chemosensors for the detection of acetylacetone and Fe^{3+}. CrystEngComm **22**, 905–914 (2020)

54. Z. Zhan, X. Liang, X. Zhang, Y. Jia, M. Hu, A water-stable europium-MOF as a multifunctional luminescent sensor for some trivalent metal ions (Fe^{3+}, Cr^{3+}, Al^{3+}), PO_4^{3-} ions, and nitroaromatic explosives. Dalton Trans. **48**, 1786–1794 (2019)

55. W.H. Huang, J. Ren, Y.H. Yang, X.M. Li, Q. Wang, N. Jiang, J.Q. Yu, F. Wang, J. Zhang, Water-stable metal–organic frameworks with selective sensing on Fe^{3+} and nitroaromatic explosives, and stimuli-responsive luminescence on lanthanide encapsulation. Inorg. Chem. **58**, 1481–1491 (2019)

56. E.L. Zhou, P. Huang, C. Qin, K.Z. Shao, Z.M. Su, A stable luminescent anionic porous metal–organic framework for moderate adsorption of CO_2 and selective detection of nitro explosives. J. Mater. Chem. A **3**, 7224–7228 (2015)

57. S. Pramanik, C. Zheng, X. Zhang, J.E. Thomas, J. Li, New microporous metal−organic framework demonstrating unique selectivity for detection of high explosives and aromatic compounds. J. Am. Chem. Soc. **133**, 4153–4155 (2011)

Authors and Affiliations

Jiewei Rong[1] · Li Li[1] · Longde Wang[1] · Wenwei Zhang[2]

✉ Jiewei Rong
  zwj0076@126.com

Wenwei Zhang
wwzhang@nju.edu.cn

[1] School of Chemical and Materials Engineering, Huainan Normal University, Huainan 232038, Anhui, People's Republic of China

[2] State Key Laboratory of Coordination Chemistry, School of Chemistry and Chemical Engineering, Nanjing University, Nanjing 210023, People's Republic of China